Bulletin of Glacier Research 16 (1998) 57–66

Melt rate of ice cliffs on the Lirung Glacier, Nepal Himalayas, 1996

Akiko SAKAI, Masayoshi NAKAWO and Koji FUJITA
Institute for Hydrospheric-Atmospheric Sciences, Nagoya University, Nagoya 464-8601 Japan

(received April 25 ; Revised manuscript received May 1, 1998)

Abstract

There are many ice cliffs exposed at the surface of debris covered glaciers. Melt rates of ice cliffs, in relation with their directions, on the Lirung Glacier were observed from May to October, 1996. Heat budget at ice cliffs was examined with the meteorological data during the observation period. Special attention was paid for the dependence of incoming shortwave radiation upon the direction of ice cliff surfaces.

Incoming shortwave radiation to a slope was estimated, taking into account the cloud intervene, from observed shortwave radiation to a horizontal surface. The calculated incoming shortwave radiation was largest at surfaces with a direction of south-east and lowest of the north-west during the monsoon season. This is because the weather is fine in the morning and the sun shines slopes which direct to the east, and it is cloudy and rainy in the afternoon and slopes which directs to the west receive relatively small solar radiation. Observed melt rate of ice cliffs coincided approximately with the calculation based on the heat balance consideration. It was 7.2 cm day^{-1} on average for cliffs with various directions during the monsoon season. The ice cliff melt amount reaches 69 % of the total ablation at debris covered area, although the area of ice cliffs occupies less than 2 % of the debris covered area.

1. Introduction

Glaciers in the Nepal Himalayas are categorized into two types, according to the surface conditions of the ablation zone : debris-free glaciers and debris -covered glaciers (Moribayashi, 1974). Almost all large valley glaciers, which are several kilometers in length, are covered with debris in their ablation zone. This type of glaciers occupy more than half of the glacialized area in the Himalayas (Moribayashi, 1974).

Nakawo *et al.* (1993) and Rana *et al.* (1997) established a model to estimate the melt rate of a debris -covered glacier by using surface temperature data from satellite images. The surface temperature on debris covered glacier depends on the debris thickness over the glacier ice. The surface topography of debris -covered glacier is very complicated and there are many ponds and ice-cliffs on debris covered glaciers. Distributions of ponds, ice cliffs and debris thickness continuously change during summer monsoon season. Thus it is necessary to consider the change of the surface condition such as the distribution of ponds or ice cliffs to estimate the growth and decay of debris -covered glacier.

Inoue and Yoshida (1980) measured the melt rate of ice cliffs with various orientations in the ablation area of Khumbu Glacier, a typical debris-covered glacier, Nepal Himalayas for one day in September, 1978. They concluded that the ablation at ice cliffs plays a very important role in the total ablation of the glacier and that the difference of incoming solar radiation to ice cliffs with various directions is a significant factor for the difference of ablation of ice cliffs. The ablation, however, was measured for one day and the solar radiation was calculated from the surface geometry and the declination of the sun following Garnier and Ohmura (1968). The effect of the clouds was not considered although rainy and cloudy days are dominant during the summer monsoon season in the Himalayas.

The melt rate in relation with the orientation of almost all ice cliffs, therefore, was measured on the ablation zone of the Lirung Glacier during the period from June to September, 1996. The observed melt rate was compared with the calculation focusing on the dependence of incoming shortwave radiation upon the orientation of ice cliffs and cloud condition.

2. Locations and observations

The observation was carried out on the debris covered ablation area of the Lirung Glacier in Langtang Valley, Nepal Himalayas 60 km north of Kathmandu, the capital city of Nepal (Fig. 1). Figure 2 shows the schematic map of the debris-covered ablation area of the Lirung Glacier and the distributions of ice cliffs and ponds.

The melt rate of one of the ice cliffs was measured with stakes at F-1 where the ice surface was almost planner. The azimuth and inclination angles of the ice cliff was 290 degrees (around NWW) and 50 degrees respectively. Two stakes were set normal to the ice surface with a string stretched between them. The melt amount was obtained from the change of the normal distance measured from the string to the ice surface. The melt rate was defined to be the vertical distance change, which are converted from the measured normal distance. Shortwave radiation income to the ice cliff was measured at an interval of 30 minutes by using pyranometer which was installed parallel to the ice surface, not horizontally.

Retreat of many ice cliffs, as a result of melting, was observed in the ablation area of the Lirung Glacier (Fig. 2). The observation was made by measuring the distance from the top edge of an ice cliff to a painted marker which was set on the debris surface behind the ice cliff, as shown in Fig. 3. The melt rate of an ice cliff was calculated from the observed retreat distance. The orientations of the cliffs were also measured several times from late August to early October.

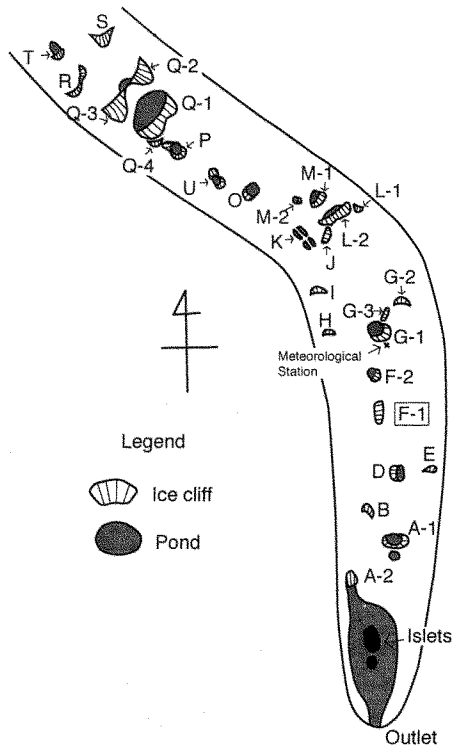

Fig. 2. The distribution of ice cliffs and ponds on the Lirung Glacier.

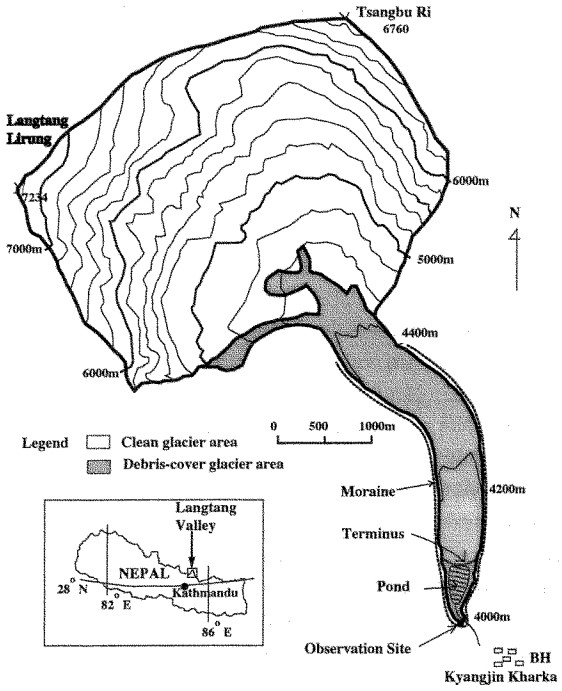

Fig. 1. Topographical map of the Lirung Glacier.

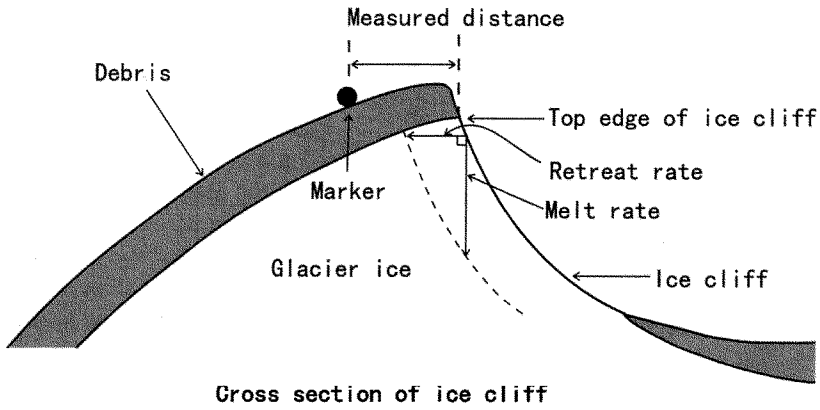

Fig. 3. Schematic diagram of the measurement for ice cliff retreat. The retreat distance of ice cliff was measured, and then it was converted into melt rate depending on the angle of the slope.

3. Meteorological conditions

A meteorological station was installed at the middle of the debris covered area of the Lirung Glacier as shown in Fig. 2, for the period from 11 May to 23 October, 1996 including the summer monsoon season. The observed elements were air temperature, relative humidity, wind speed, surface temperature of the supraglacial debris layer, downward and upward solar radiation and net radiation. They were measured at an interval of 5 minutes for the whole observation period. The details of the observation and the preliminary results were described by Fujita *et al.* (1997).

Figure 4 shows the diurnal change of solar radiation and precipitation which were averaged hourly during the observation period. The figure also shows the calculated solar radiation at the top of the atmo-

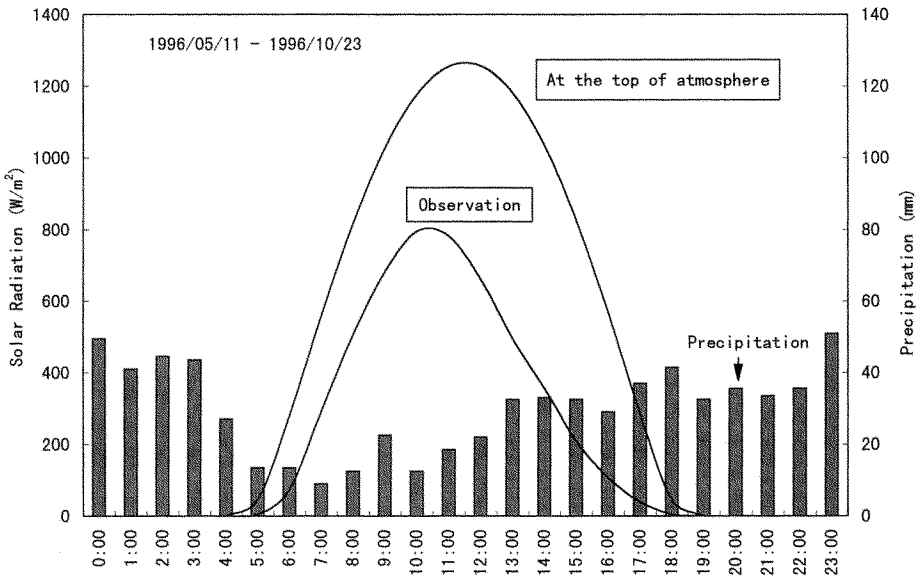

Fig. 4. Hourly average of observed shortwave radiation and hourly total of precipitation, together with the calculated shortwave radiation at the top of the atmosphere, during the observation period from May 5 to October 23 in 1996.

sphere. The observed solar radiation is smaller than the calculated solar radiation by the effect of the turbidity of the atmosphere and cloud intervene. It was relatively fine in the morning with small amount of precipitation and strong solar radiation. The difference between the calculated radiation for the top of the atmosphere and the observed one was small, at most 400 Wm^{-2}. From the noon, on the other hand, precipitation was large in association with low solar radiation, and the difference of the radiations was large : *e.g.* about 650 Wm^{-2} at 2 PM. The observed solar radiation was largest at 10 AM, with relatively small cloud amount in the morning, although solar radiation was largest at noon at the top of the atmosphere. The precipitation continued toward nighttime.

4. Calculation for ice cliff melting

4.1. Incoming shortwave radiation to a sloped surface

Considering the effect of cloud intervene the incoming solar radiation to a sloped surface for a sloped unit area was expressed as follows (Garnier and Ohmura, 1968) :

$$I_d' = I_o \cos(X \wedge S). \quad (1)$$

Where, I_d' = solar radiation on a given slope for a sloped unit area,
I_o = observed solar radiation at a horizontal plane,
X = a unit coordinate vector normal to the slope and pointing away from the ground,
S = a unit coordinate vector expressing the height and position of the sun, and
$\wedge$ = a symbol denoting the angle between X and S.

Equation (1) can be expressed by trigonometrical function as follows,

$$I_d' = I_o\{[(\sin\phi \cos H)(-\cos A \sin Z_x) - \sin H (\sin A \sin Z_x) + (\cos\phi \cos H)\cos Z_x]\cos\delta + [\cos\phi(\cos A \sin Z_x) + \sin\phi \cos Z_x]\sin\delta\}. \quad (2)$$

Where, ϕ = the latitude of the slope,
H = the hour angle measured from solar noon,
A = the azimuth of the slope direction, measured clockwise from north,
Z_x = the zenith angle of the vector X, and
δ = the sun's declination, positive when the sun is north of the equator.

Figure 5 shows the incoming shortwave radiation toward a unit sloped area without the effect of the cloud nor the scatter in the atmosphere averaged for the observation period. It decreases with increasing the angle of slope for a given azimuth angle as shown in Fig. 5. For a certain slope angle, the incoming solar radiation is relatively large at around west and east. Steep slopes receive larger solar radiation than gentle slopes when the solar elevation is low in the morning or evening. This should accelerate the melting of steep slope facing toward either east or west.

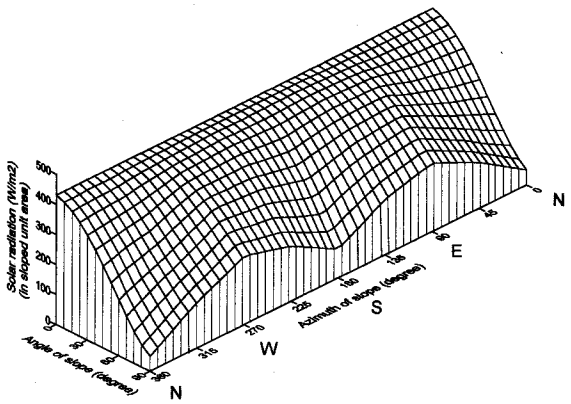

Fig. 5. The relation between the calculated incoming shortwave radiation and the slope orientation for unit sloped area without considering the cloud effect nor the scattering in the atmosphere.

The incoming solar radiation to a sloped surface was converted to the radiation for a unit horizontal area with the following equation derived from equation (1) :

$$I_d = I_o \cos(X \wedge S) \cdot \frac{1}{\cos Z_x}, \quad (3)$$

where, I_d = solar radiation on a given slope for a unit horizontal area.

The solar radiation for a horizontal surface at the top of the atmosphere, I_{th} is compared in Fig. 6 with observed solar radiation at the meteorological station, I_o. The observed solar radiation, I_o is much smaller than I_{th}, fluctuating significantly, owing to the clouds intervene and turbidity of the air.

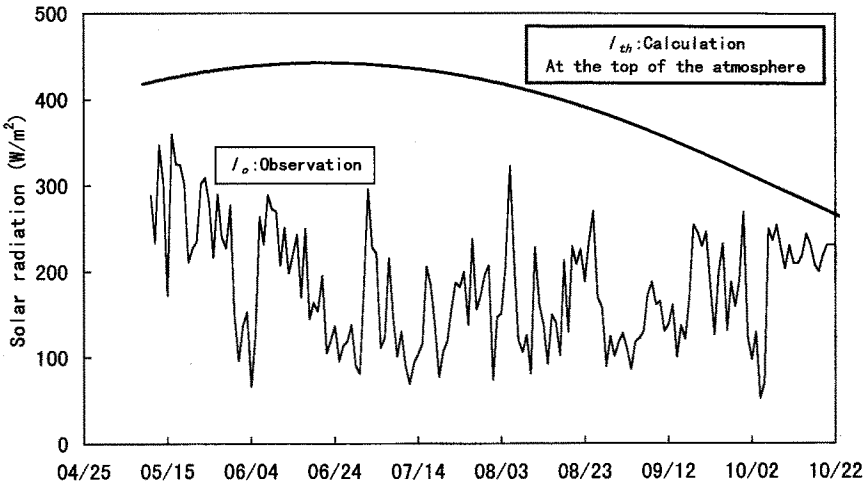

Fig. 6. Observed shortwave radiation at the glacier surface, and the shortwave radiation at the top of the atmosphere from May 5 to October 23 in 1996.

Figure 7 shows the dependence of shortwave radiation for a unit horizontal area on the orientation of slopes. Figure 7(a) is essentially the same as Fig. 5 except the radiation is expressed not for a sloped unit area but for a unit horizontal area, which is called I_{td}. I_{td} increases generally with the increase of inclination angle, and the trend is remarkable when the inclination approaches toward 90°. This is mainly caused by the fact that the area of sloped ice surface corresponding to a unit horizontal area, increases with the increase of inclination angle. I_{td} has two symmetric peaks at west and east, because the solar radiation should be the same either when the sun is rising or sinking. At the glacier surface, however, one peak is found for the shortwave radiation to a sloped surface for a unit horizontal area, I_d around the south-east and no peak around west (Fig. 7(b)).

Cross section of Fig. 7 for azimuth angles of north, east, south and west are selected and shown in Fig. 8, where I_{td} for ice cliffs facing to east and west is completely the same, and lowest for cliffs to north (Fig. 8(a)). As shown in Fig. 8(b), however, I_d is largest for cliffs to east and second largest to the south. West facing cliffs receive smaller amount of radiation than that facing to south. I_d for north facing cliffs, which is the smallest, decreases with increasing inclination.

The average inclination angle of ice cliffs in the Lirung Glacier was around 50°, for which the incoming shortwave radiation is larger than horizontal ice surfaces when the azimuth is south or east as shown in Fig. 8(b).

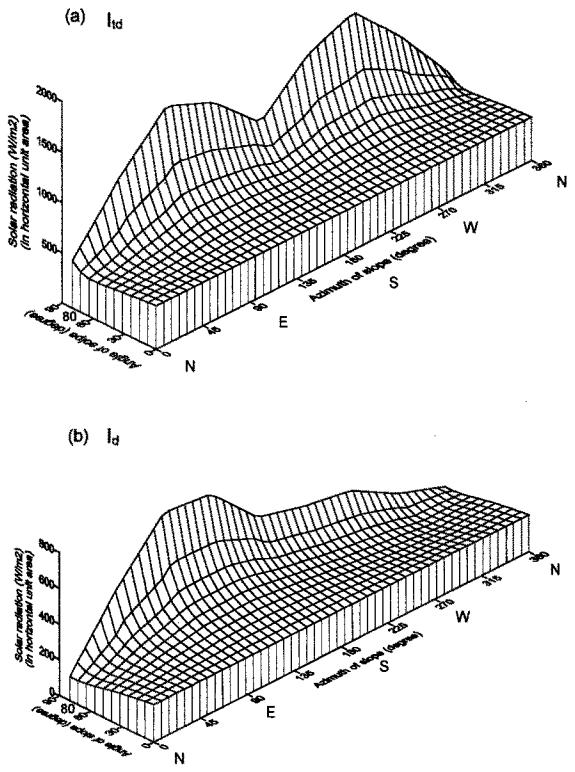

Fig.7. Shortwave radiation depending on the orientation of the slope converted plotted for unit horizontal area (a) : at the top of the atmosphere : I_{td}, and (b) : at the glacier surface : I_d. The difference between (a) and (b) gives the effect of cloud and air turbidity in the atmosphere. (The coordinate axes of angle of slope and azimuth of slope are opposite to Fig.5.)

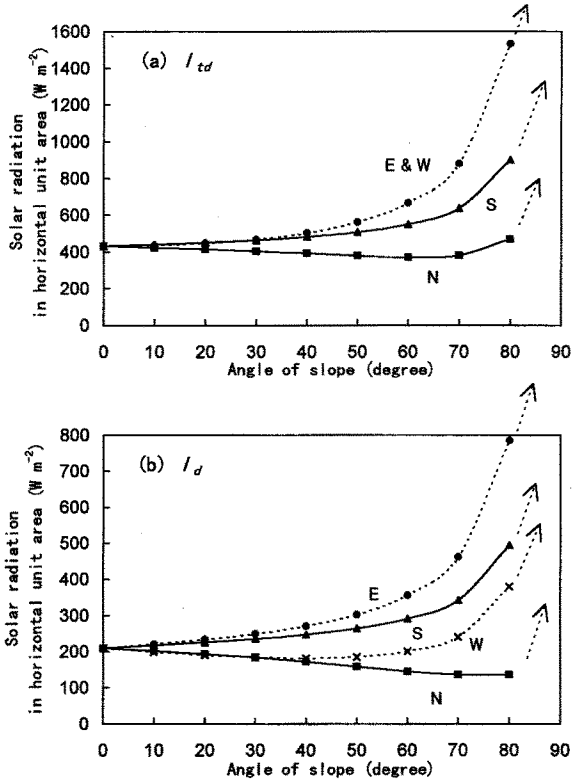

Fig. 8. (a) : The dependence of shortwave radiation for unit horizontal area on inclination angle of the slope, with azimuth angle of north, south, east and west : at the top of the atmosphere. (b) : at the glacier surface.

The different feature between I_{td} and I_d is due to the diurnal change of cloud condition during the summer monsoon season. The slope with the azimuth of east receives relatively high solar radiation with little cloud in the morning. Thereafter, it becomes cloudy and begins raining in the afternoon. The slopes, whose azimuth is between south and west, receive smaller solar radiation due to much cloud in the afternoon.

The diffuse solar radiation was not taken into account in the above calculation. The above feature of the radiation dependence on the orientation of cliff walls, however, would generally hold, since the direct radiation is very large in the Himalayas.

4.2. Heat balance calculation for ice cliff melting

Heat input to an ice surface, Q_s [Wm^{-2}] can be calculated with the following heat balance equation :

$$Q_s = \sum^{t}(I+R+H+E),$$

(4)where, I = net shortwave radiation [Wm^{-2}],
R = net longwave radiation [Wm^{-2}],
H = turbulent sensible heat flux [Wm^{-2}] and
E = turbulent latent heat flux [Wm^{-2}].

All fluxes were taken positive when they are toward the ice surface.

The net shortwave radiation coming into an ice surface was calculated by :

$$I = (1-\alpha)I^{\downarrow}, \tag{5}$$

where, $I^{\downarrow}$ = Downward shortwave solar radiation [Wm^{-2}] ,and
α = Observed albedo of the ice surface [0.11].

Incoming shortwave radiation to a slope (I_d) in unit horizontal area were considered in downward shortwave radiation $I^{\downarrow}$ in the Equation (3).

Net radiation, downward and upward shortwave radiations and surface temperature were observed at the meteorological station. Downward longwave radiation was estimated, using the following equation, from the observation for the site, where the glacier surface was covered with a thick debris layer,

$$R^{\downarrow} = NR - I + \sigma T_{ms}^4, \tag{6}$$

where, $R^{\downarrow}$ = downward longwave radiation [Wm^{-2}],
NR = net radiation [Wm^{-2}],
σ = Stefan-Boltzmann constant [5.67×10^{-8} Wm^{-2} K^{-4}] and
T_{ms} = surface temperature at the site of the meteorological station [K].

It was assumed that the downward longwave radiation was uniform for the whole glacier, including ice cliffs in the ablation zone, since the longwave radiation from the debris surface facing to the cliffs was relatively small. Thus, net longwave radiation incoming to the ice surface is expressed as :

$$R = R^{\downarrow} - \sigma T_s^4, \tag{7}$$

where, T_s = surface temperature of the ice cliffs [273 K].

Sensible and latent heat fluxes were calculated by the bulk aerodynamic formula presented by Kojima (1979), which was established for snow surfaces :

$$H = 3.60\,U(T_a - T_s), \tag{8}$$

$$E = 2.31\times10^{-3} lU(e_a - e_s), \quad (9)$$

where, U = wind speed [m sec^{-1}],
T_a = air temperature [K],
l = latent heat for vaporization [2.50×10^6 Jkg^{-1}],
e_a = vapor pressure of air [hPa] and
e_s = vapor pressure at ice surfaces [hPa].

The value e_s was assumed to be the saturated vapor pressure at ice surface temperature T_s = 273 K.

The melt rate of ice cliffs was estimated from the above heat balance calculation, taking into account the incoming shortwave radiation for respective azimuth and inclination angles of ice cliffs. The meteorological station on the glacier located at around the middle part of the glacier at about 4200 m a.s.l., and the relative height of the cliffs from the meteorological station was roughly 200 m at most. The relative height difference leads to differences in sensible and latent heat by less than 20 Wm^{-2}, depending on the temperature lapse rate. It was assumed, therefore, that sensible and latent heat fluxes were uniform for the whole ablation area and calculated with data at the meteorological station.

5. Results and discussions

5.1. Incoming shortwave radiation to ice cliffs

Daily averaged shortwave radiation income was calculated for an ice cliff surface at site F-1, using Equation (3), as shown in Fig. 9. The figure also shows the observed shortwave radiation. The both are plotted for unit horizontal area. The observed radiation was almost always higher than the calculated value by 10-50 Wm^{-2} during the summer monsoon season. It would be due to the effect of the diffuse solar radiation, which was not taken into consideration in the calculation.

5.2. Heat balance of the ice cliff

The daily averaged heat balance elements are shown in Fig. 10 for the ice cliff F-1 from May to October. It was assumed that the surface temperature of the ice cliff was at the melting point, though it could be lower than the melting point in May and October from night to morning.

It shows that shortwave radiation is most important as Inoue and Yoshida (1980) described. It was in the range of 100 to 300 Wm^{-2} in our observation.

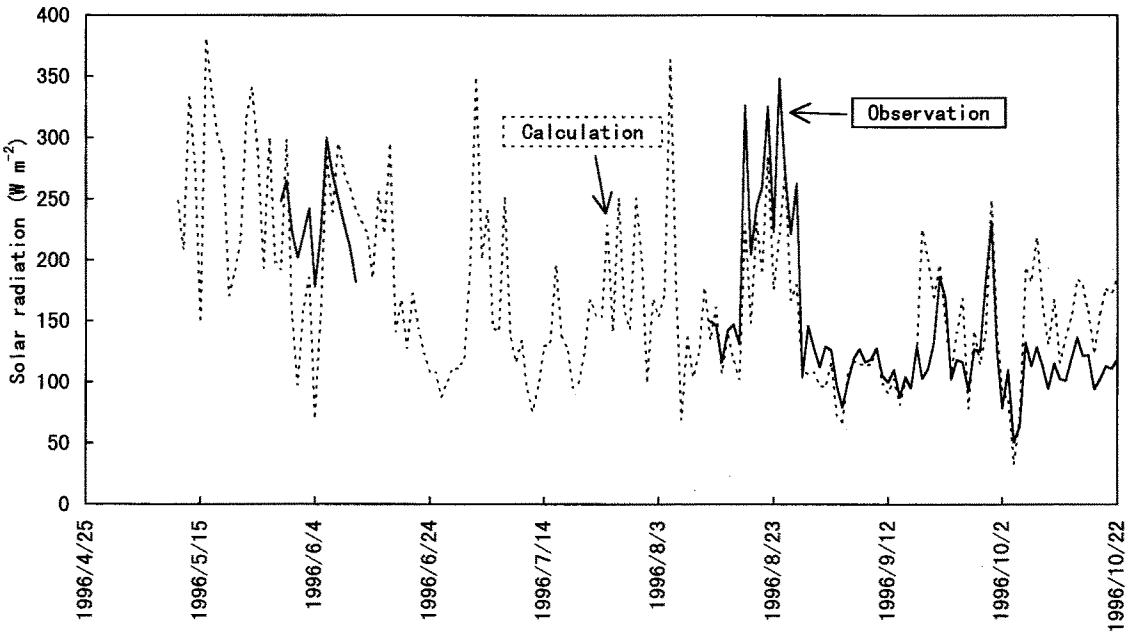

Fig. 9. Calculated and observed shortwave radiation at site F-1 during the observation period.

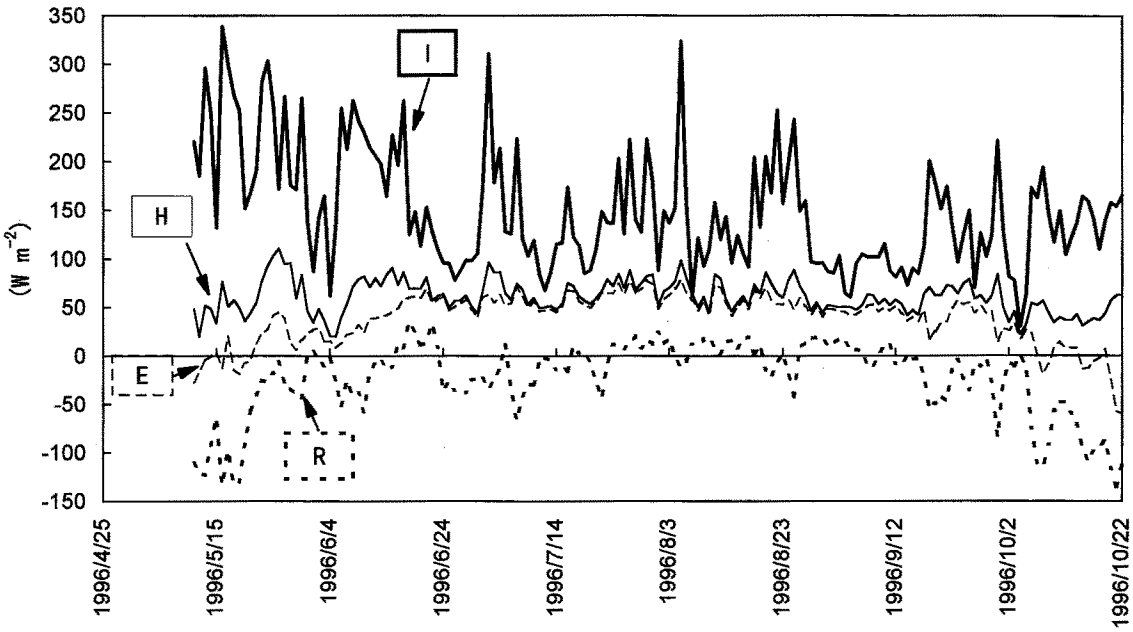

Fig. 10. Elements of heat balance at ice cliff at site F-1 during the observation period.

Sensible and latent heats were comparatively small, only from 50 to 100 Wm^{-2}, although they contributed some during the summer monsoon season. Longwave radiation was not significant either for ice cliff melting, when the longwave radiation from the debris surface facing to an ice cliff was measured, which account for the longwave radiation approximately 50 Wm^{-2}.

5.3. Melt rate of the ice cliffs

Figure 11 shows the daily observed and calculated vertical melt rates at ice cliff F-1. The calculation is based on Equations from (1) to (9). They are compared favorably in general. There is a tendency that the observed melt rate is smaller than calculated value during the summer monsoon season, though the diffuse-beam shortwave radiation income was not taken into account in the calculation. The observed melt rate tend to be larger than that of calculated in September during post-monsoon season. It is considered that the first cause for the difference would be the change of ice surface albedo, which is dependent on the abundance of particles from a debris layer on the ice cliff with melt water. The second cause could be the difference in the surface boundary layer in the atmosphere above the debris covered glacier : the bulk constant for turbulent fluxes could be different. The rough topography of the debris-covered glacier may cause complicated turbulent wind.

Figure 12 shows the averaged observed melt rate from June to October for ice cliffs with various azimuth and inclination angles, where the melt rate is given in vertical direction. The melt rate was calculated for a cliff with the inclination angle of 50°, the average of the observed cliff slopes. The result is also shown in the figure. The observed melt rates have large difference with the calculated melt rate. This could be due to the fact that the observed ice cliffs have various angle of slope, and the local wind speed may be different from place to place. The smallest slope angle of ice cliffs was approximately 30° and more gentle slopes than 30° were covered with debris. The observed points in the azimuth of around north are comparatively larger in number than that of around south, since many ice cliffs direct to around north in the Lirung Glacier.

The averages of melt rate and the azimuth angle of all observed ice cliffs were 7.2 cm day^{-1}. The ice

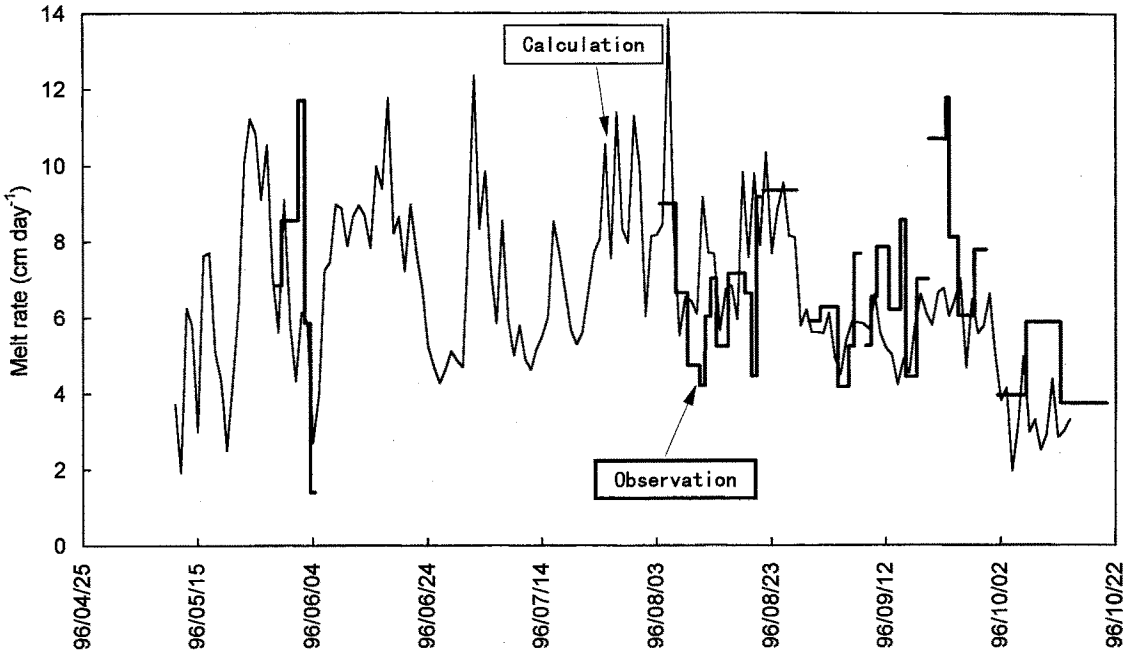

Fig. 11. Calculated and observed melt rate at site F-1 during the observation period.

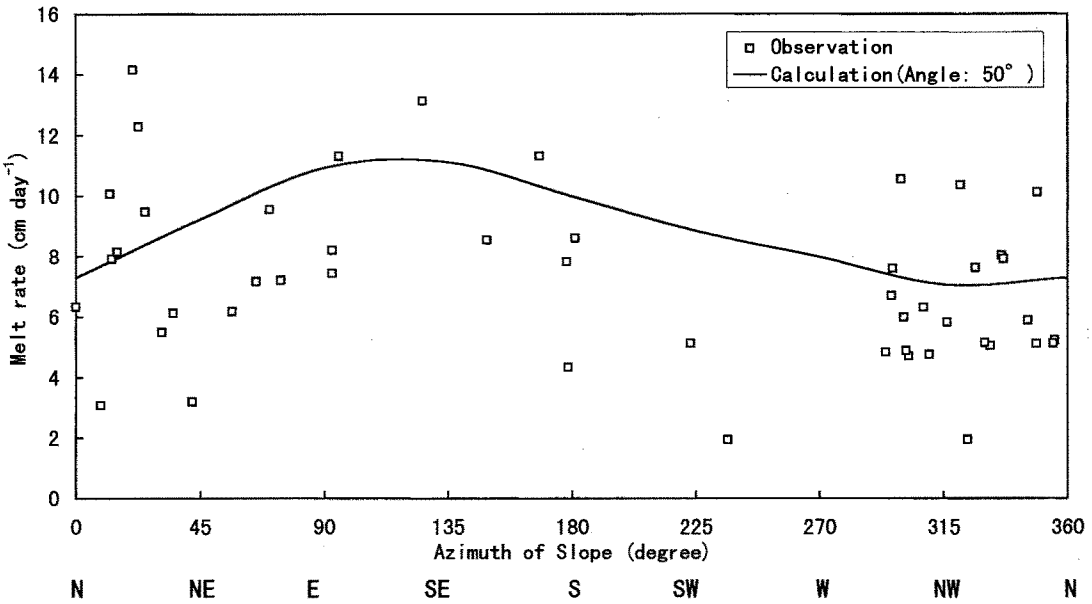

Fig. 12. Calculated melt rate of ice cliffs where slope angle is fixed 50°and observed melt rate of ice cliffs with various azimuths, for the whole observation period.

cliff area was measured to be 0.04 km^2 in the horizontal projection in the whole debris covered area(2.2 km^2 (Rana, 1997)) of the glacier. The average melt rate was estimated by Rana(1997) to be 0.19 cm day^{-1}, which includes the melt rate of ice for the observation period. Therefore, the melting ice cliff is very significant, accounting for 69 % of the whole ablation amount of the debris covered area.

Concluding remarks

To estimate the melt rate of ice cliffs with various direction, incoming shortwave radiation for a sloped surface was calculated, taking into account the effect of the cloud intervene.

Incoming shortwave radiation was relatively large to slopes with south-east direction, and small for those with in north-west direction, because the weather was fine in the morning and rainy in the afternoon during the summer monsoon season. In particular ice cliffs with azimuth from south to east received larger shortwave radiation than that with horizontal surface for unit horizontal area.

Calculated melt rate approximately corresponded well with observed melt rate, presumably because the shortwave radiation is the major heat source for melting.

The average melt rate in the debris covered area was estimated about 0.19 cm day^{-1} during observation period by Rana (1997). The average melt rate at ice cliffs, 7.2 cm day^{-1} is more than 30 times larger than the average for the debris area. As a result of that the melt amount of the ice cliff is 69 % of the whole debris covered area, though the ice cliff area is only 1.8 % of the debris covered area. It is certain that the ice cliffs plays an important rule in the ablation and the change of surface geometry of debris covered glaciers.

Acknowledgments

We would like to express our thanks to the Department of Hydrology and Meteorology, Ministry of Water Resources, His Majesty's Government of Nepal. We thank all of the members of the Project for their kind support in the field. The expenses for the field research and for data analyses were supported by a Grant-in-Aid for Scientific Research (Project No. 06041051 and No. 09490018) from Ministry of Education, Science, Sports and Culture, Japanese Government.

References

1. Fujita, K., Sakai, A. and Chhetri, T.B. (1997) : Meteorological observation in Langtang Valley, Nepal Himalayas, 1996. Bull. Glacier Res., **15**, 71-78.
2. Garnier, B.J. and Ohmura, A. (1968) : A method of calculating the direct shortwave radiation income of slopes. Journal of Applied Meteorology, **7**, 796-800.
3. Inoue, J. and Yoshida, M. (1980) : Ablation and heat exchange over the Khumbu Glacier. Seppyo, **41**, Special Issue, 26-33.
4. Kojima, K. (1979) : Snow melting process and heat budget, Kishokenkyu Note, Meteorological Society of Japan, **136**, 1-38. (In Japanese)
5. Moribayashi, S. (1974) : On the characteristics of Nepal Himalayan Glaciers and their recent variation. Seppyo, **36**, 11-21. (In Japanese with English sbstract)
6. Nakawo, M., Moroboshi, T. and Uehara, S. (1993) : Satellite data utilization for estimating ablation of debris covered glaciers. IAHS Publ., **218**, 75-83.
7. Rana, B. (1997) : Study on glacier ablation under debris-cover for runoff modeling of a river basin in Langtang Valley, Nepal Himalaya. Ph.D. thesis, Nagoya University, 157p.
8. Rana, B., Nakawo, M., Fukushima, Y. and Ageta, Y. (1997) : Application of a conceptual precipitation-runoff model (HYCYMODEL) in the debris-covered glacierized basin in the Langtang Valley, Nepal Himalaya. Annals of Glaciology, **25**, 226-231.